nature COMMUNICATIONS

ARTICLE

https://doi.org/10.1038/s41467-019-13742-w OPEN

Measuring local-directional resolution and local anisotropy in cryo-EM maps

Jose Luis Vilas[1], Hemant D. Tagare[2], Javier Vargas[3], Jose Maria Carazo[1*] & Carlos Oscar S. Sorzano[1*]

The introduction of local resolution has enormously helped the understanding of cryo-EM maps. Still, for any given pixel it is a global, aggregated value, that makes impossible the individual analysis of the contribution of the different projection directions. We introduce MonoDir, a fully automatic, parameter-free method that, starting only from the final cryo-EM map, decomposes local resolution into the different projection directions, providing a detailed level of analysis of the final map. Many applications of directional local resolution are possible, and we concentrate here on map quality and validation.

[1] Biocomputing Unit, Centro Nacional de Biotecnologia (CNB-CSIC), Campus Universidad Autonoma, 28049 Cantoblanco, Madrid, Spain. [2] Department of Biomedical Engineering, Yale University, New Haven, CT 06520, USA. [3] Department of Anatomy and Cell Biology, McGill University, Montreal H3A 0G4, Canada. *email: carazo@cnb.csic.es; coss@cnb.csic.es

Once a map is reconstructed, its resolution is estimated to avoid possible over-interpretations. Resolution can be determined in a global or in a local manner. The global one is a single parameter that determines the degree of reliability of the whole map; being the FSC the most common (for a review of resolution measures see ref. [1]). In contrast, local approaches determine this reliability voxel by voxel through different approaches as windowed FSC between two halves[2], or the detection of structural features above the noise level[3,4].

The need for local resolution approaches emerges as a consequence of multiple effects happening at the sample at the imaging and processing levels, such as: existence of sample heterogeneity, flexibility, wrong angular assignment of single particles, bad angular coverage of the projection sphere, existence of preferred directions or radiation damage among others. Local resolution maps may quantify the combined effect of all these limiting factors into the final cryoEM map; however, they are not able to isolate the effect of each factor alone. Recent works like the 3DFSC[5] or the efficiency[6] have tried to address individually some of these problems introducing the concept of directional resolution. However, these approaches were intrinsically global, determining a merit function that informs on the existence of a bad angular coverage. Local measures of these effects have not been studied yet, being this issue one of the goals of our study and, up to our knowledge, the first time directionality and locality have been brought together. In this work, a local-directional resolution measurement approach is proposed. We will show here that, as opposed to just local resolution methods[2–4], by expanding the concept of (voxel) locality by performing a complete "directional local resolution" analysis, other way to analyze the informational content of a cryo-EM map emerges, opening many new possibilities, from map validation and quality control to chain tracing, among others. This article focuses on some of the suggested quantitative indicators of map quality assessment. In all cases we want to note two important points: (1) that the single input to our method is the final cryo-EM map, without any knowledge of the original particles or their assigned projection directions, (2) that our approach rests on the strong mathematical framework of monogenic signals[7], building on MonoRes[4] (see Methods section).

The new algorithm, that we call MonoDir, calculates the local resolution along a set of directions in 3D (see Methods section). In essence, given a voxel location ($\mathbf{r}$), we calculate the contribution to its aggregated local resolution of the information coming from each direction. In other words, each location (voxel) will have associated to it a set of resolution values equal to the number of analyzed directions; they are called local directional resolution values. Note that, essentially, what we are doing is to treat local resolution not just as a single "value", the directional resolution operator assigns a real number to every direction at every voxel, the changed is, therefore, of a very fundamental mathematical nature (thus it is a function on the product space $\mathbb{R}^3 \times RP^2$ where the $\mathbb{R}^3$ component is the voxel and the RP^2 component is the direction. Previously defined local resolution operators are functions only on $\mathbb{R}^3$. Extending the notion of local resolution to $\mathbb{R}^3 \times RP^2$ is the main contribution of this paper.). Consequently, it is no wonder that MonoDir offers the possibility to analysis cryo-EM maps from totally new perspectives, much beyond the limited set of examples we present in this work, all oriented towards map validation.

The simplest quality indicators we can think of are "the Highest (e.g., 3 Å) and Lowest (e.g., 10 Å) local-Directional Resolutions Maps". The highest resolution map informs about the highest resolution value, $H(\mathbf{r})$, for each pixel, $\mathbf{r}$, without taking into account the direction along which that resolution is measured. Similarly, the lowest resolution map can be obtained with the corresponding lowest resolution values, $L(\mathbf{r})$. In general, the highest and lowest resolution directions do not need to be orthogonal to each other. To get statistically "robust" maps, the values of $L(\mathbf{r})$ and $H(\mathbf{r})$ are considered as the percentiles 0.05 and 0.95, respectively, of the resolution distribution of all possible directions.

The next indicator that we have introduced is "the Average Directional Resolution" (ADR). It only requires the detection of the direction contributing to the highest resolution $H(\mathbf{r})$ (and which is this maximum resolution value) and, in the same way, to the lowest resolution $L(\mathbf{r})$, both in the robust statistical sense previously mentioned. The ADR is mathematically defined as:

$$\mathrm{ADR}(\mathbf{r}) = \frac{L(\mathbf{r}) + H(\mathbf{r})}{2}. \quad (1)$$

The ADR provides valuable information about the map quality and informs about the possible existence of preferred directions. However, to infer this information it is required the local resolution map to compare with, the ADR map by itself is not a local anisotropy metric. In a way, it is like a local resolution map weighted by the local anisotropy. Note that when the values $L(\mathbf{r})$ and $H(\mathbf{r})$ are similar, it means that the map presents a low local resolution anisotropy, and therefore all directions exhibit the same quality. In contrast, if there is local anisotropy, the value of the lowest resolution will be substantially smaller than the one of the highest resolution, making the mean lower. To complement ADR and getting an estimator of resolution anisotropy, a dispersion metric is introduced, thus, for each voxel we introduce a statistically robust metric, the half interquartile range between the 0.17 and 0.83 percentiles (these percentiles are selected to represent an unit of standard deviation when the distribution is normal). It is reminded that for each voxel, MonoDir computes the local-directional resolution for a set of directions; therefore, there exists as many local-directional resolutions as number of computed directions. The percentiles are calculated from this distribution of local-directional resolutions. It must be highlighted that as dispersion metric, the half interquartile range is therefore our proposed metric for measuring the local resolution anisotropy.

Obviously, the ADR and the half interquartile range inform about the resolution anistropy, but they do not inform about which are the preferred directions. However, this piece of information can be very easily measured by introducing a modification of the otherwise classical plot of projection directions. The new plot will be referred to as polar plot and it represents the number of voxels that have their highest resolution along a specific direction. In other words, the polar plot represents a histogram of the highest local-directional resolution values on the projection sphere, where the number of counts along each direction is represented by the size of the dot, see an example in Fig. 1. Thus, we are capable of identifying not only situations of systematic lack of particle views (as normal polar plots do), but errors in angular assignment as well. Indeed, if our 3D alignment algorithm had incorrectly assigned to a certain projection direction images that were really coming from a different direction, this error will introduce blurring in the map along that direction and, consequently, the number of voxels with the highest resolution will decrease. Therefore, our new angular plot should present an uniform coverage of the projection sphere for isotropic maps, otherwise we either have a lack of projection directions or a bad angular assignment.

MonoDir computes the local-directional resolution map along a certain set of directions. However, it is also possible to analyze the local directional resolution along particular directions that may be related to critical characteristics of the map. In this context, it is specially interesting to analyze resolution along two directions connected to a polar decomposition of the map: the radial and tangential directions. In the case of the calculation of the radial local resolution, for each point of the map we calculate the direction of a line joining that point to the center of the map, and we calculate the local resolution along this direction, see Supplementary Fig. 1. For the case

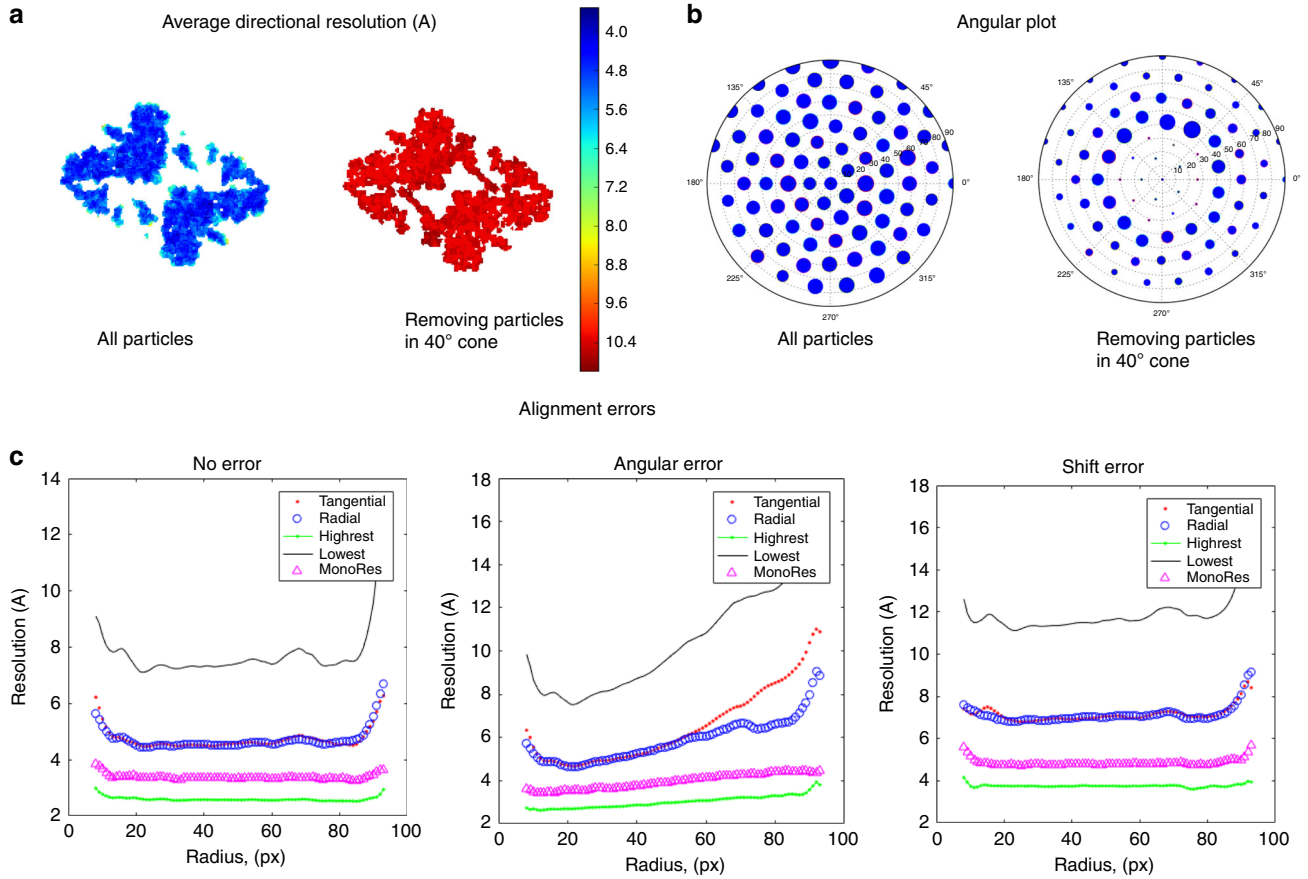

Fig. 1 Results from a computer simulated map from the beta-galatosidase. The atomic model PDB-3j7h was converted into a density map, first for maps obtained considering all projection directions and then with missing directions, showing (**a**) Average Directional Resolution (ADR), (**b**) angular plot, (**c**) radial average of local-directional resolution maps (tangential-pink points, radial-blue circles, as well as lowest and highest) when: random angular errors of standard deviation of 1.2 degrees, random shift errors of standard deviation of 1 degrees, and error free reconstructions are considered.

of the tangential resolution, at each point in the map we calculate its tangential plane and we average all directional resolutions in that plane. The expectation is that these directions would be particularly sensitive to errors in angular alignment, specially when resolution along those directions is plotted along radii. Specifically, an approximately linear relation between radius and radial average of resolution can be observed, being the slope related to the angular error in the angular alignment (as expected by simple geometrical considerations, at least for the tangential resolution). This is described in depth in the Supplementary Information. Note that angular plot and the radial average resolution curves show global information about the reconstructed map, but it would never obtained without calculating first the associated local directional information.

Results

Local-resolution anisotropy: synthetic map. We first tested MonoDir in a synthetic fully controlled setting, using the structural model of β-galactosidase corresponding to PDB entry 3*j7h*[8,9]. The aim of this synthetic example is to illustrate in a detailed manner the information that MonoDir provides. Thus, the atomic model was first converted into an electron density map[10] and a gallery of 500 random projections was obtained with known angular assignments; Gaussian noise with zero mean and standard deviation of 2 a.u. was then added. We performed two experiments with these data, the results are presented in Fig. 1. The first experiment aimed at simulating the case of having preferred orientations on the cryo-EM grid, so we removed all particles with tilt angles smaller than 40 degrees (missing cone). The lack of information along the missing directions naturally introduced a resolution anisotropy in the map. Moreover, MonoDir works by establishing statistical tests to elucidate if the local energy of signal is higher than the energy of noise. Along the missing cone direction, there is nothing to compare, and the resolution assigned is the lowest possible. The second experiment obtained the reconstructed structure without removing any particle orientation, this experiment addressed the relationship between the radial profiles of radial and tangential resolution and the presence of alignment errors. In this way, we analyzed these plots for the cases of exact refinement (no errors), in-plane shift errors only, and, finally, angular errors only.

To start with the ADR, the values were clearly different between the map reconstructed from all particles Fig. 1a and the one obtained in the case of a missing angular gap Fig. 1a. As expected, the value of ADR was much lower in the presence of anisotropy than in its absence. Then, we tested the behavior of the new polar plot of projection directions, showing the number of voxels with the highest resolution per direction Fig. 1b. Clearly, the plot in (1b), corresponding to the case with no angular gap (b-on the left), is much more even than the case showing an angular projection gap (b-right). In the latter case the angular gap, forming a cone of 40 degrees, is very clear in the center of the plot (the projection directions around the missing cone have a somehow exaggerated number of voxels with the highest resolution, an effect we have noticed in transition regions and obviously is a consequence of the synthetically-imposed missing cone, therefore, this effect should not occur in experimental cases).

Finally, the plots of radial and tangential resolutions per radius are very informative of alignment errors and confirm our previously

introduced expectations; to test this issue, the known angular assignment of particles and shift were randomized around the true direction; a Gaussian distribution with a standard deviation of 1.2 degrees was considered for the angular assignment and a standard deviation of 1 pixel for the shift. In this way, the plot corresponding to the case of not having errors in the assignment of projection directions Fig. 1 (c, left) shows flat profiles and a highest directional resolution close to Nyquist. Then, the plot where only shift errors were introduced Fig. 1 (c, center) also have flat profiles, but with values shifted to lower resolutions. Finally, when angular errors were introduced, a clear slope appears Fig. 1 (c, right), indicating the existence of angular errors (and their importance—larger errors induce a larger slope). Note the similar behavior of the tangential and radial resolutions at lower radii, roughly corresponding to the maximum sphere fully contained inside the macromolecule, while they diverge beyond this point, with the tangential resolution normally having a higher slope. It is also very clear how both the lowest and highest directional resolution estimations also follow a clear slope with the radius, being MonoRes estimation always close to the maximum resolution, although lower (a logical behavior considering how it is defined).

Local-resolution anisotropy: experimental maps. We start with the case of two data sets, the 20S Proteasome[11] (EMDataBank: EMDB-6287) and the 80S Ribosome[12] (EMDB-2275), which are shown side by side in Fig. 2. Starting with the ADR (Fig. 2a), the values for the proteasome all over the map are much lower than those for the ribosome, indicating that the proteasome map is much more isotropic. The comparison between ADR values and the FSC also support this observation, since they are similar to the reported FSC resolution of 2.8 Å (at 0.143); in addition, another indicator, the 3DFSC[5] (see Supplementary Figures) also indicates isotropy. On the contrary, the case of the ribosome is totally different, with a

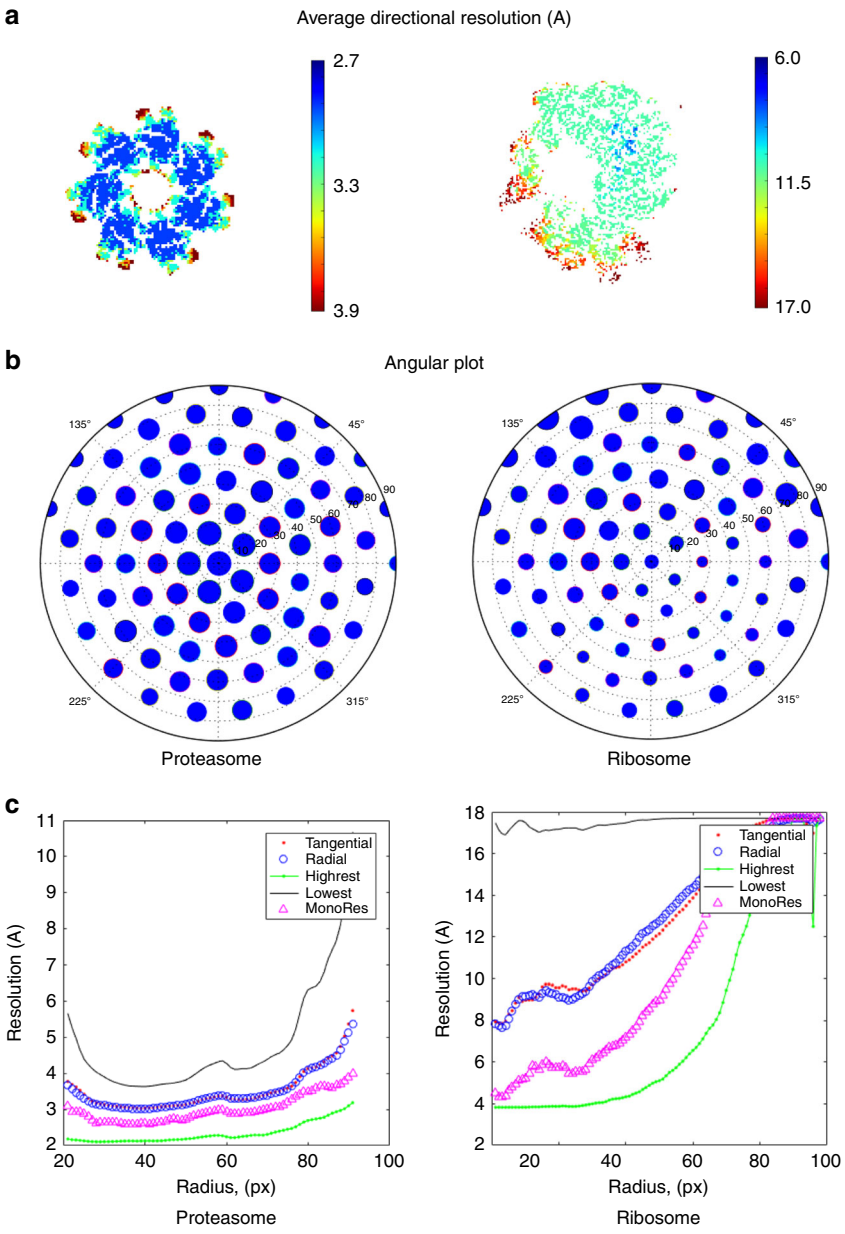

Fig. 2 Results for proteasome 20S and ribosome 80S. a Average Directional Resolution (ADR), (**b**) polar plot, and (**c**) radial average of local tangential (pink points) and radial (blue circles) directions plotted along radii, together with the highest (green points), lowest (black continuous) and MonoRes (violet triangles) local resolution estimations.

wide dispersion of ADR values. Then, polar plots for directional distribution of particles (Fig. 2b) show a quite even distribution for the proteasome, but a very uneven distribution of highest resolution directions for the ribosome. Finally, note that plots of radial and tangential resolutions along radii are very informative (Fig. 2c), with those coming from the proteasome presenting a quite small slope—an indicator of a good angular assignment—while those calculated for the ribosome show a very high slope. We note that this ribosome sample was also used as example in ref. [6], reaching also the conclusion that the angular alignment was imperfect, but the new insight is that we have been able to prove it without any knowledge of the original images or their angular assignment (as the method in ref. [6] needed).

The last experimental example of MonoDir application is presented in Fig. 3. In this case, the specimen on the left and right columns is the same, Influenza Hemagglutinin (HA) trimer[5], for

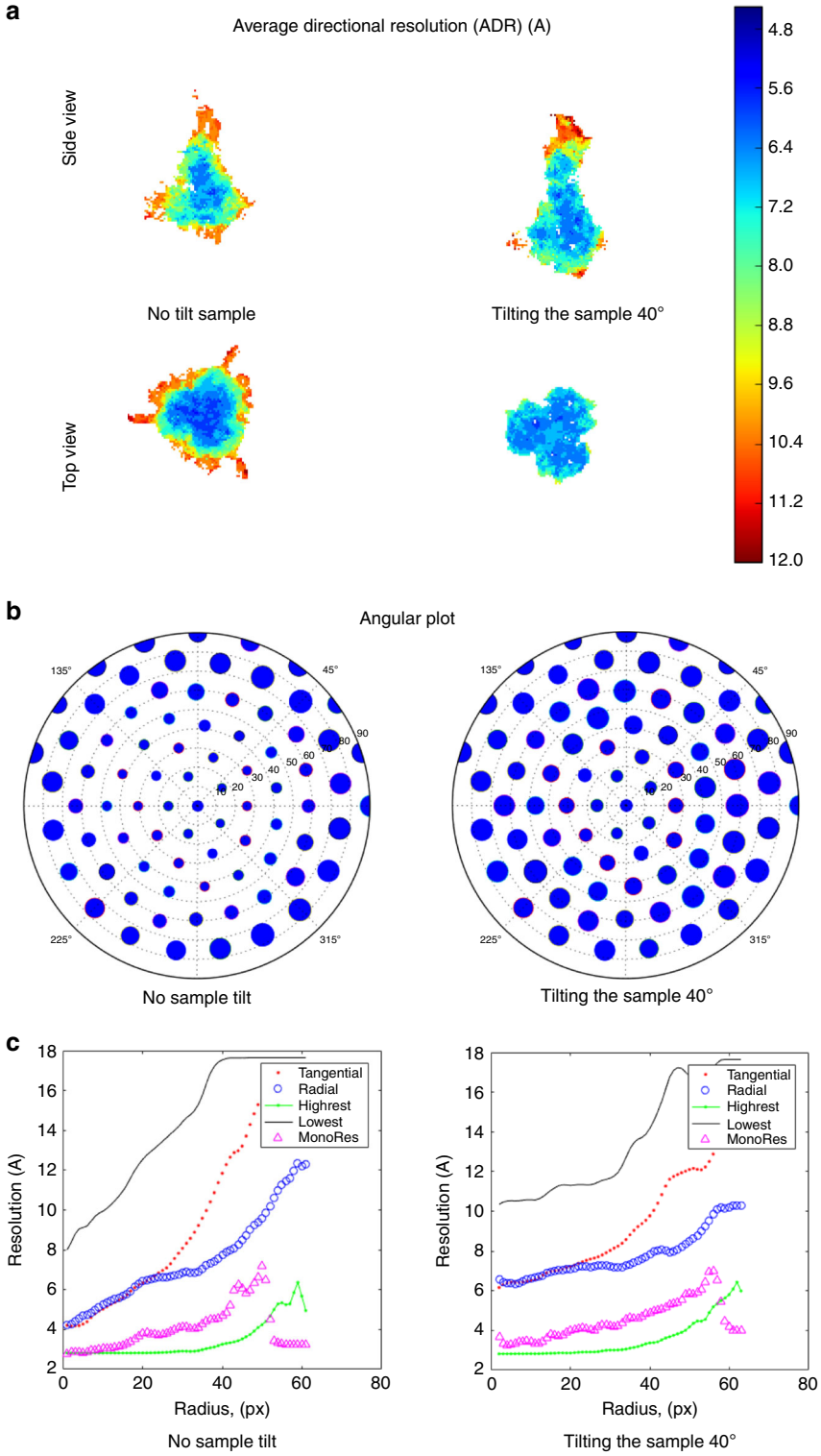

Fig. 3 Results for Influenza Hemagglutinin (HA) trimer when the sample is untilted and tilted. a ADR, (**b**) angular plot, and (**c**) radial averages as in Fig. 1.

which two maps were deposited (unfiltered maps at 0 and 40 degrees in EMPIAR entries 10196, 10197, respectively), the first one was strongly affected by the presence of preferred orientations, while this handicap was greatly minimized in the second map by tilting the EM grid. It is clear in Fig. 3a, left uncorrected map, right corrected, that ADR values are higher for the uncorrected map than for the corrected one. The success of the map correction was initially supported by the 3DFSC[5] (see Supplementary Figures 3DFSC and dispersion). The polar angular distribution plots (Fig. 3b) exhibit a non-uniform distribution of highest local-directional resolutions, indicating the existence of preferred directions, top views in this case. In contrast, for the tilted sampled, the same plot presents a more uniform local-directional resolution coverage of the projection sphere, although with a slight but not negligible non-uniform coverage inside a central cone. Finally, radial plots of radial and tangential resolutions (Fig. 3c) indicate a higher slope for the uncorrected map than for the corrected map, exactly as expected.

Discussion

We have further expanded the concept of "local resolution" to "directional local resolution", where the contribution to the local resolution estimation associated to different directions is individually analyzed. The concept of resolution depends not only on the map position, but having different values at different directions. This fact adds a new dimension to the capacity to study a cryo-EM map. In this article we have introduced some "map quality indicators", but many more could be imagined, and in completely different application domains, such as, automatic chain tracing or quality checks within iterative angular alignment algorithms. We present, therefore, a very general tool and its initial application to map validation, but we expect this tool to have a much wider impact in cryo-EM.

We have also shown how the use of local-directional measurements provide new information about the quality of the reconstructed map, identifying angular alignment errors and the existence of preferred directions and resolution anisotropy; moreover, this information is extracted from the reconstructed map, without the need to access the original set of images or any other information related to them (this is a unique and very strong feature of *MonoDir* that no other methods posses). Regarding the capacity of *MonoDir* to identify alignment errors, we have presented clear examples in which the slope of radial plots of both tangential and radial can be qualitatively related to the existence of higher of lower angular errors, providing a unique guidance tool that did not exist in the field before. Furthermore, in Supplementary Information we have analyzed more in-depth this effect, proving that the approximation to a linear behavior between alignment error and tangential and radial resolution slopes indeed hold, although more work is need to fully characterize this effect, probably analyzing scaling terms not yet taken into account, so that ultimately we could provide with a quantitative description of this relationship.

In conclusion, the set of examples analyzed in this work with *MonoDir* represent a proof of concept of how important is to treat local resolution not as a scalar but as a directional measurement. In all cases *MonoDir* was able to provide a new view of the cryoEM map, helping us to understand better its quality by providing an unprecedented level of detail regarding the source of the possible errors affecting the map. In this respect, we consider that the possibilities of "directional local resolution" are only starting, and that future works will propose novel extensions applicable to many areas of work in the field.

Methods

MonoDir algorithm. The root of *MonoDir* is *MonoRes*[4] in which an estimation of the monogenic signal and its local amplitude at different frequencies was used to determine by an hypothesis test on the cryo-EM map whether signal (macromolecular structure) estimation is significantly higher than noise estimation at any given frequency. A mask allows to discriminate between noise and protein. To measure local-directional resolution maps and, therefore, anisotropy, a directional filter must be previously applied.

Our goal was to filter directionally the electron density map and then to calculate the local resolution of the directional-filtered map obtaining the so-called local-directional resolution map. In Supplementary Figures a scheme of the measurement process is shown. The directional filter is defined by determining the Fourier Transform of the volume and masking the Fourier Transform with a cone that only keeps the frequencies inside it. The cone axis is arranged along the direction in which the local-directional resolution is calculated, and the cone angle is set by the user (in our examples we used 30 degrees). By computing the inverse Fourier Transform, a directional filtered map is obtained.

We then measured the local resolution of these directionally-filtered maps using *MonoRes*[4]. MonoRes computes the local amplitudes of noise and signal. Unfortunately, despite using smooth filters in Fourier space, the directional filtering introduced some ringing, in particular around the borders and in the plane perpendicular to the measured direction. This ringing might modify the noise statistics. To avoid that, the original MonoRes algorithm was modified. These modifications can be found in the Supplementary Information.

The process of measuring local-directional resolution is repeated until we have covered the full projection sphere. In our examples, we computed 81 directions with an angular sampling of 15 degrees. Once all directions were analyzed, the local-directional resolution information is combined to produce the different outputs (lowest, highest, radial/tangential resolution maps, and the local average directional resolution map).

Data availability

All published data sets used in this paper were taken from the Electron Microscopy Data Bank (https://www.ebi.ac.uk/pdbe/emdb/) and, their entries are: EMD-2984, EMD-2275, EMD-6287, and EMD-8731 (last one also in EMPIAR (https://www.ebi.ac.uk/pdbe/emdb/empiar/) entries 10097 and 10096).

Code availability

MonoDir is publicly available in Xmipp[13] and has been integrated in Scipion[14] (http://scipion.cnb.csic.es).

Received: 6 June 2019; Accepted: 18 November 2019;
Published online: 02 January 2020

References

1. Sorzano, C. O. S. et al. A review of resolution measures and related aspects in 3D Electron Microscopy. *Progress Biophys. Mol. Biol.* **124**, 1–30 (2017).
2. Cardone, G., Heymann, J. B. & Steven, A. C. One number does not fit all: mapping local variations in resolution in cryo-EM reconstructions. *J. Struct. Biol.* **184**, 226–236 (2013).
3. Kuculkelbir, A., Sigworth, F. J. & Tagare, H. D. Quantifying the local resolution of cryo-EM density maps. *Nat. Methods* **11**, 63–65 (2014).
4. Vilas, J. L. et al. MonoRes: automatic and accurate estimation of local resolution for electron microscopy maps. *Structure* **26**, 337–344 (2018).
5. Tan, Y. Z. et al. Addressing preferred specimen orientation in single-particle cryo-EM through tilting. *Nat. Methods* **14**, 793–796 (2017).
6. Naydenova, K. & Russo, C. Measuring the effects of particle orientation to improve the efficiency of electron cryomicroscopy. *Nat. Commun.* **8**, 629 (2017).
7. Unser, M., Sage, D. & Van De Ville, D. Multiresolution monogenic signal analysis using the Riesz-Laplace wavelet transform. *IEEE Trans. Image Process.* **18**, 2402–2418 (2009).
8. Bartesaghi, A. et al. Structure of β-galactosidase at 3.2-A resolution obtained by cryo-electron microscopy. *PNAS* **111**, 11709–11714 (2014).
9. Bartesaghi, A. et al. 2.2 Å resolution Cryo-Em structure of beta-galactosidase in complex with a cell-permeant inhibitor. *Science* **348**, 1147 (2015).
10. Sorzano, C. O. S. et al. Fast and accurate conversion of atomic models into electron density maps. *AIMS Biophys.* **2**, 20150102 (2015).
11. Campbell, M. G., Veesler, D., Cheng, A., Potter, C. S. & Carragher, B. 2.8 Å resolution reconstruction of the Thermoplasma acidophilum 20S proteasome using cryo-electron microscopy. *Elife* **4**, e06380 (2015).
12. Bai, X. C., Fernandez, I. S., McMullan, G. & Scheres, S. H. W. Ribosome structures to near-atomic resolution from thirty thousand cryo-EM particles. *Elife* **2**, e00461–e00461 (2013).

13. de la Rosa-Trevín, J. M. et al. Xmipp 3.0: an improved software suite for image processing in electron microscopy. *J. Struct. Biol.* **184**, 321–328 (2013).
14. de la Rosa-Trevin, J. M. et al. Scipion: a software framework toward integration, reproducibility, and validation in 3D electron microscopy. *J. Struct. Biol.* **195**, 93–99 (2016).

Acknowledgements

J.M.C. thanks Dr. Richard Henderson for discussions in the context of the use of radial and tangential resolution maps. J.L.V., J.M.C., C.O.S.S. were supported by the Spanish Ministry of Economy and Competitiveness through Grants BIO2016-76400-R(AEI/FEDER, UE), the "Comunidad Autónoma de Madrid" through Grant: S2017/BMD-3817, and the use of resources of Instruct-ERIC. H.D.T. was supported by NIH grant R01GM114051. J.V. was supported by grants from NSERC Discovery Grant (RGPIN-2018-04813) and FRQNT New University Researchers Start-Up (NC-253837). European Union (EU) Horizon 2020 through grants EOSC Life (INFRAEOSC-04-2018, Proposal: 824087), HighResCells (ERC - 2018 - SyG, Proposal: 810057).

Author contributions

J.M.C., C.O.S.S., J.V., H.D.T. developed the idea of measuring local directional resolution. J.M.C. suggested the application for finding error alignments. J.M.C., C.O.S.S., J.V., H.D.T., and J.L.V. defined metrics for measuring local anisotropy resolution. J.L.V. and C.O.S.S. introduced the angular plots for measuring preferred directions. J.L.V. and C.O.S.S. wrote the code in Xmipp and the implementation in Scipion.

Competing interests

The authors declare no competing interests.

Additional information

Supplementary information is available for this paper at https://doi.org/10.1038/s41467-019-13742-w.

Correspondence and requests for materials should be addressed to J.M.C. or C.O.S.S.

Peer review information *Nature Communications* thanks Alexis Rohou and the other, anonymous, reviewer(s) for their contribution to the peer review of this work.

Reprints and permission information is available at http://www.nature.com/reprints

Publisher's note Springer Nature remains neutral with regard to jurisdictional claims in published maps and institutional affiliations.

Supplementary Information: Measuring local-directional resolution and local anisotropy in cryo-EM maps

J.L. Vilas et al.

Supplementary Information

Supplementary Note 1: Modifications on MonoRes core for MonoDir algorithm

The non-directional *MonoRes* algorithm computes the non-directional local resolution of a given map by means of statistical tests at different frequencies. The method begins by high pass filtering the map with center frequencies ranging from low to high, and calculating the local monogenic amplitudes of the map at the center frequency. *MonoRes* statistical tests attempt to determine if the local amplitudes at the filtering frequency are significant higher than the 95th percentile of the distribution of noise. If they are, then the voxel is declared to have significant amplitude at the filtering frequency. The highest filtering frequency at which a voxel has significant amplitude is declared to the local resolution of the voxel. The distribution of noise is calculated by considering all voxels outside a particle mask. To avoid the existence of false positive, a local resolution value is assigned to a voxel when the hypothesis test fails consecutively twice, being the assigned resolution value is the last frequency that passed the hypothesis test.

To introduce directional measures, the input map is directionally filtered along of a set of directions that cover the projection sphere. The directional filter is carried out in Fourier space by means of cones. Thus, for each directionally filtered map the estimation of local resolution maps can be performed by applying *MonoRes*. Unfortunately, the use of directional filters introduces artifacts that might affect to the local resolution that *MonoRes* will estimate. This kind of artifact is due to the filter-ringing that the directional filter generates. There are two critical modifications:

1) The particle radius of the protein is initially determined (radius of the sphere that contains the whole protein). Then, to obtain the noise statistics, we only look outside of this sphere, see Suppl Fig. 2.

2) All points inside the shell are not valid, note that directional filters introduce a ringing in the orthogonal direction to the filtering direction. Therefore, the distribution of noise is estimated in the intersection of the shell with the cone defined by the filtering direction. See Suppl Fig. 2.

Other modifications of the *MonoRes* algorithm were carried out in terms of performance. Note that to compute the resolution anisotropy, it is necessary to apply *MonoRes* as many times as the number of analyzed directions. As a consequence, *MonoRes* algorithm was carefully re-implemented and adding a thread parallelization in an efficient manner.

Supplementary Note 2: Angular assignment errors

In the main text it was shown how the radial averages of radial and tangential resolution can be used to identify angular assignment errors in the reconstructed maps. However, it remains to relate the slope of the radial average and the committed error. To do that, two atomic models were considered, the first one was the $\beta-$galactosidase [4] with pdb entry $5a1a$ and the second one was the ribosome [5] with pdb entry $5wf0$. Both models were converted into density maps using [6] and a set of 500 projections were generated with a sampling rate of 1 Å/pixel. Then, noise was added to the set of projections with zero mean and standard deviation of 2 a.u. Because of the way projections were generated, the angular orientation of the set of particles is well known. However, to introduce angular assignment errors, the angles were randomized following a normal distribution with a given standard deviation. The choice of this standard deviation establishes the angular assignment error, note that the 99% of the distribution will be in the interval $[-3\sigma, 3\sigma]$ (if $\sigma = 1$ degree, the maximum committed error will be 3 degrees). Thus, synthetic maps reconstructed with angular assignment errors corresponding with $\sigma = 1, 1.5, 2, 2.5, 3$ degrees were considered and evaluated with *MonoDir*.

The analysis of the angular assignment error is carried out with the radial average curves. In Fig. 6 the *MonoDir* results for the radial and tangential components are shown. Note that the higher σ (angular assignment error), the greater slope of the radial average curves.

In Suppl. Fig. 6(a) the results with $\beta-$galactosidase can be observed. Figure shows that the behaviour of the radial averages of the radial and tangential components is different. In particular, both curves diverges at specific radius, in particular at 20px, 40px and 60 px. This is easily explained considering the shape of the protein. The reason for these divergences is the macromolecule geometry, see Suppl. Fig. 7. The $\beta-$galactosidase has a hole with radius of 20px in the center and, therefore, the region 0-20 px does not have structural meaning. From 20 px to 40 px, there exist voxels with structure along all possible directions and, in this region, the radial averages present a linear behaviour. However, when the radius is greater than 40 px, and because the structure is very elongated, there is no structure for averaging along one of the axis, and therefore, the radial resolution cannot be measured properly. The results is that the radial average curve is affected, changing its behaviour. The same scenario occurs at 60 px, which represents the second divergence point of the radial averages. The conclusion we derive from these experiments is very simple: protein geometry affects the radial averages, so that the slopes of these curve must be measured in those regions in which there is mass essentially in all directions, which ensure the proper measurement of the radial component responsible of this effect. Summarizing, the deviations from the linear behaviour of the radial average curve for the radial and tangential resolutions are due to the protein geometry. To check that, the structure of the ribosome was chosen because it is relatively homogeneus in all directions. Furthermore, to reduce possible problems with the measurement of the radial resolution component, the 500 particles were circularly masked (with radius 80 px), ensuring that inside the circle there always exists informational content, then noise was added and the map reconstructed. In Suppl. Fig. 6(b) the radial averages of the masked ribosome as result of *MonoDir* are shown. Note that the geometry of the masked ribosome is spherical and therefore, the radial average curve does not present deviations from the linear behaviour (effect of the protein geometry). Moreover, and as expected, the radial and tangential resolution radial averages curves are essentially the same curve.

Taking into account this information, a linear model is proposed for the loss of resolution, $R_\sigma(r)$ in terms of the radius for the radial average curves as it follows

$$R_\sigma(r) = R_0 + K(\sigma)r,$$

where r represents the radius, σ the angular uncertainty or error, and R_0 and $K(\sigma)$ the intercept term and the slope (that depends on the angular uncertainty σ). Hence, a linear regression to the radial and tangential radial averages was carried out for each reconstructed maps with $\sigma = 1, 1.5, 2, 2.5, 3$, the goal is to relate these uncertainties with the slope of the radial average. In Tables. 1 and 2 the slopes and intercept terms of the linear fittings for the $\beta-$galactosidase and the ribosome are respectively summarized. Considering the effect of the protein geometry, the regression were carried out in the intervals $[20, 0]$ px and $[20, 60]$ $\beta-$galactosidase and the ribosome respectively. It is observed that the higher slope, the higher angular error. In contrast, the intercept terms seems to be constant.

Finally, we wanted to determine the exact relation between the slopes and the committed error in the alignment process. Unfortunately, this seems to depend on the specific macromolecule. However, a simple linear model can also be proposed for which

$$K = m\sigma, \tag{1}$$

σ	K_r	$R_{0,r}$	R^2	K_t	$R_{0,t}$	R^2
1.0	0.0120	4.77	0.98	0.0094	4.84	0.90
1.5	0.0245	4.57	0.99	0.0186	4.72	0.97
2.0	0.0334	4.43	0.99	0.0321	4.41	0.99
2.5	0.0502	4.23	0.99	0.0489	4.17	0.99
3.0	0.0658	4.03	0.98	0.0562	4.18	0.99

Supplementary Table 1 – Summary of the linear fitting of the radial and tangential radial average curves of the $\beta-$galactosidase supplementary example. The table shows the slope K, the intercept term, R_0 and the coefficient of determination R^2. The subindex r and t denotes the radial and tangential components.

σ	K_r	$R_{0,r}$	R^2	K_t	$R_{0,t}$	R^2
1.0	0.0149	4.25	0.98	0.0118	4.39	0.99
1.5	0.0237	4.18	0.99	0.0193	4.34	0.99
2.0	0.0354	4.03	0.99	0.0296	4.22	0.99
2.5	0.0435	4.06	0.99	0.0377	4.24	0.99
3.0	0.0498	4.11	0.98	0.0437	4.27	0.99

Supplementary Table 2 – Summary of the linear fitting of the radial and tangential radial average curves of the Ribosome supplementary example. The table shows the slope K, the intercept term, R_0 and the coefficient of determination R^2. The subindexes r and t denotes the radial and tangential components.

with m a proportionality constant and K the measured slope from the radial average curves (radial or tangential). This linear fitting can be seen in Suppl. Fig. 8, and it obeys the linear equations $K = 0.0267\sigma - 0.0161$ and $K = 0.0179\sigma - 0.0024$ for the $\beta-$galactosidase and the ribosome respectively. Despite these linear regressions seems to be enough good, their slopes, m are different ($m = 0.0267$ and $m = 0.0179$), and therefore a hidden mechanism, probably some form of yet unknown normalization, must finally establish the exact relation between the slope of the radial averages curves and the committed error int he alignment process. The analysis of this hidden mechanism will be part of a future work.

1 Supplementary figures

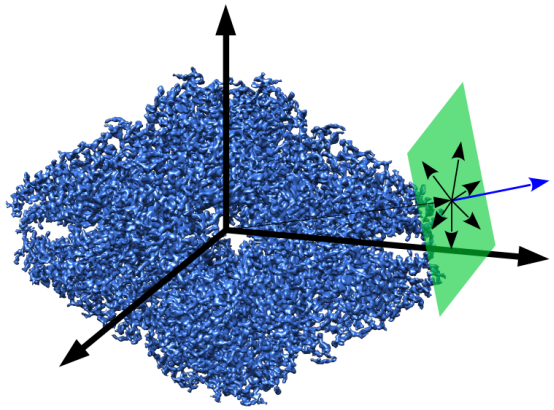

Supplementary Figure 1 – **(Supplementary) Radial an tangential resolution measurement**. For each voxel, the radial vector and a set of tangential vector are calculated. The local resolution corresponding to those vectors are calculated. By averaging the tangential resolutions the tangential component is calculated.

Supplementary References

[1] C. O. S. Sorzano, J. Vargas, J. Oton, V. Abrishami, J. M. de la Rosa-Trevin, J. Gomez-Blanco, J. L. Vilas, R. Marabini, J. M. Carazo, "A review of resolution measures and related aspects in 3D Electron Microscopy", Progress in Biophysics and Molecular Biology, **124**, 1-30 (2017).

[2] J. L. Vilas, J. Gomez-Blanco, P. Conesa, R. Melero, J. M. de la Rosa Trevın, J. Oton, J. Cuenca, R. Marabini, J. M. Carazo, J. Vargas, C. O. S. Sorzano, "MonoRes: automatic and accurate estimation of local resolution for electron microscopy maps", Structure 26, 337–344, (2018).

[3] Y.Z. Tan, P.R. Baldwin, J.H. Davis, J.R. Williamson, C.S. Potter, B. Carragher, D. Lyumkis, "Addressing preferred specimen orientation in single-particle cryo-EM through tilting", Nature Methods, 14, 793-796 (2017).

[4] A. Bartesaghi, A. Merk, D. Matthies, X. Wu, J. Milne, S. Subramaniam, "2.2 ÅResolution Cryo-Em Structure of Beta-Galactosidase in Complex with a Cell-Permeant Inhibitor", Science, 348, 1147 (2015).

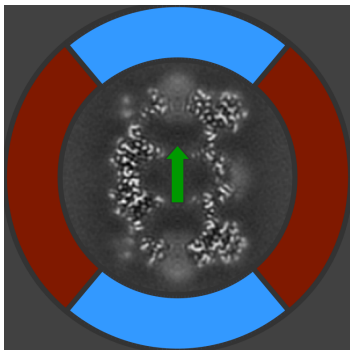

Supplementary Figure 2 – **(Supplementary) Scheme of MonoDir noise estimation area**. Given a measurement direction (green arrow), the noise in calculated in a shell greater than the particle radius. To avoid directional filtering artifacts only the intersection of a cone along the filtering direction with the shell is used to estimate the noise (blue area)

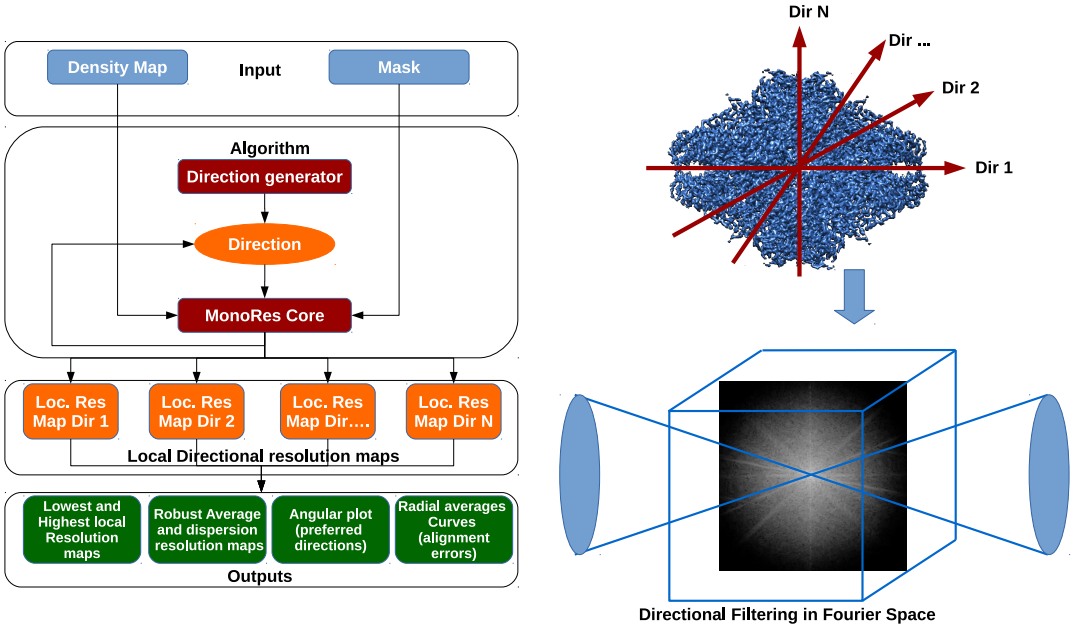

Supplementary Figure 3 – **(Supplementary) Scheme of MonoDir local-directional resolution estimation**.

[5] M. Fislage, J. Zhang, Z.P. Brown, C.S. Mandava, S. Sanyal, M. Ehrenberg, J. Frank, "Cryo-EM shows stages of initial codon selection on the ribosome by aa-tRNA in ternary complex with GTP and the GTPase-deficient $EF-Tu^{H}84A$", Nucleic Acids Research, 46, 11, 5861-5874, (2018)

[6] C.O.S. Sorzano, J. Vargas, J. Oton, V. Abrishami, J.M. de la Rosa-Trevin, S. del Riego, A.

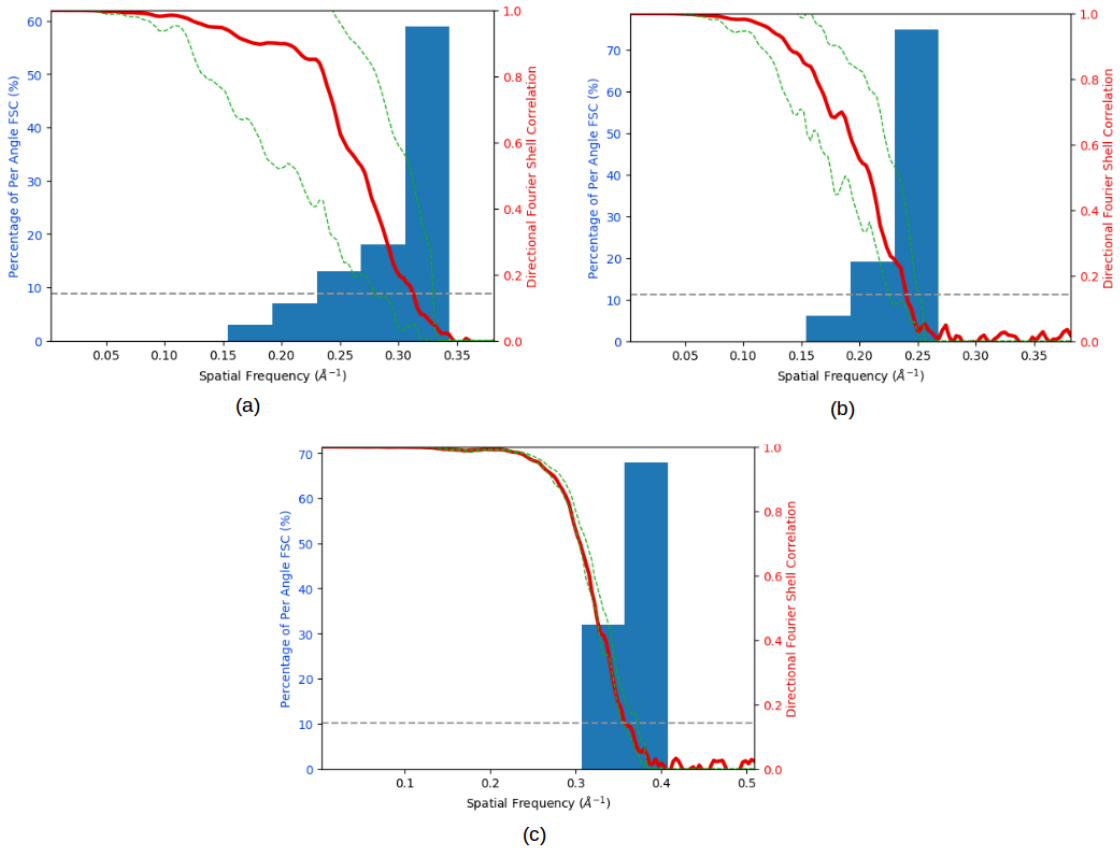

Supplementary Figure 4 – **(Supplementary) Results of the 3DFSC [3]** for the Influenza Hemagglutinin (HA) trimer when the sample is (a) untilted,(b) tilted 40 degrees, and (c) The proteasome 20S.

Fernandez-Alderete, C. Martinez-Rey, R. Marabini, J.M. Carazo, "Fast and accurate conversion of atomic models into electron density maps", AIMS Biophysics, 2, 20150102, (2015)

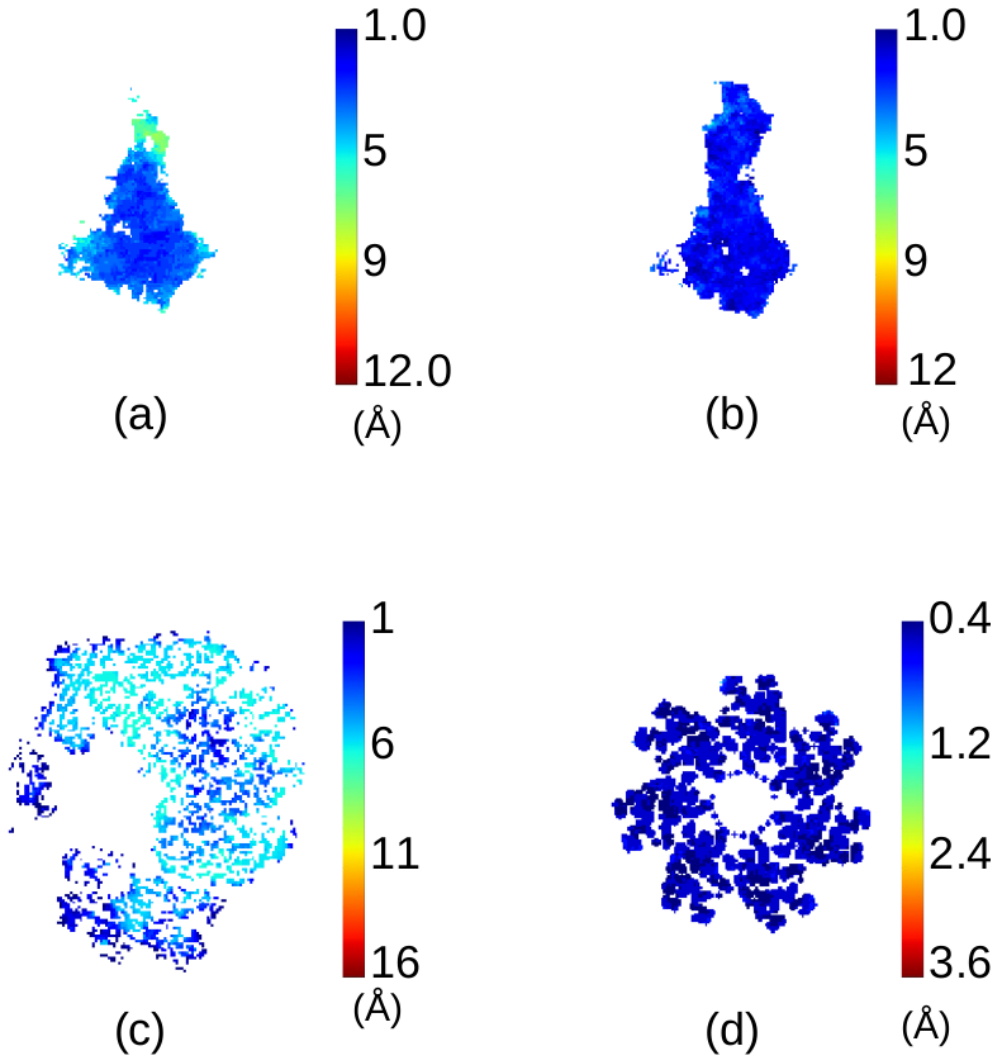

Supplementary Figure 5 – **(Supplementary) Interquartile measures of local-directional resolution for Influenza Hemagglutinin (HA) trimer** when the sample is (a) untilted,(b) tilted 40 degrees (c) ribosome 70S and (d) proteasome 20S.

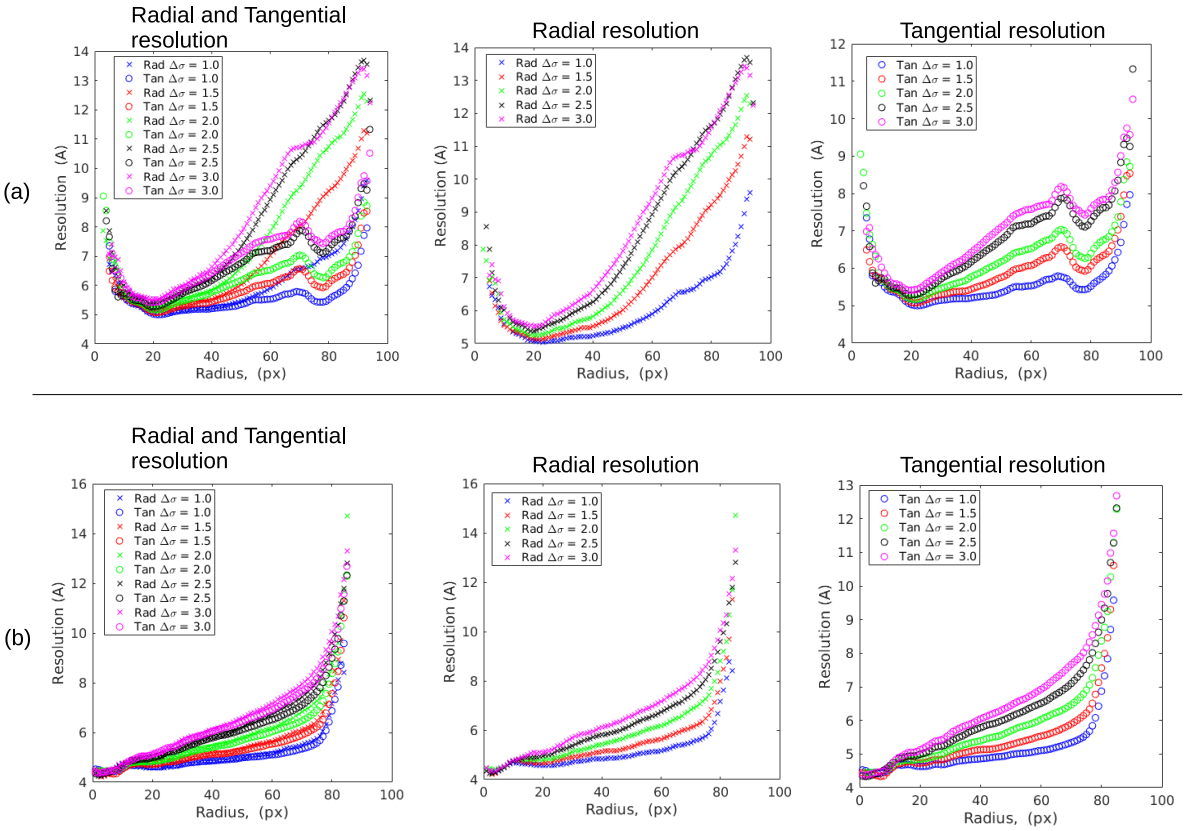

Supplementary Figure 6 – **(Supplementary) Radial average curves of the radial (Rad) and tangential (Tan) resolution considering several angular errors** with $\sigma = 1, 1.5, 2, 2.5, 3$ degrees, for the (a) and $\beta-$galactosidase map from pdb entry $5a1a$ and (b) Ribosome map from pdb entry $5wf0$.

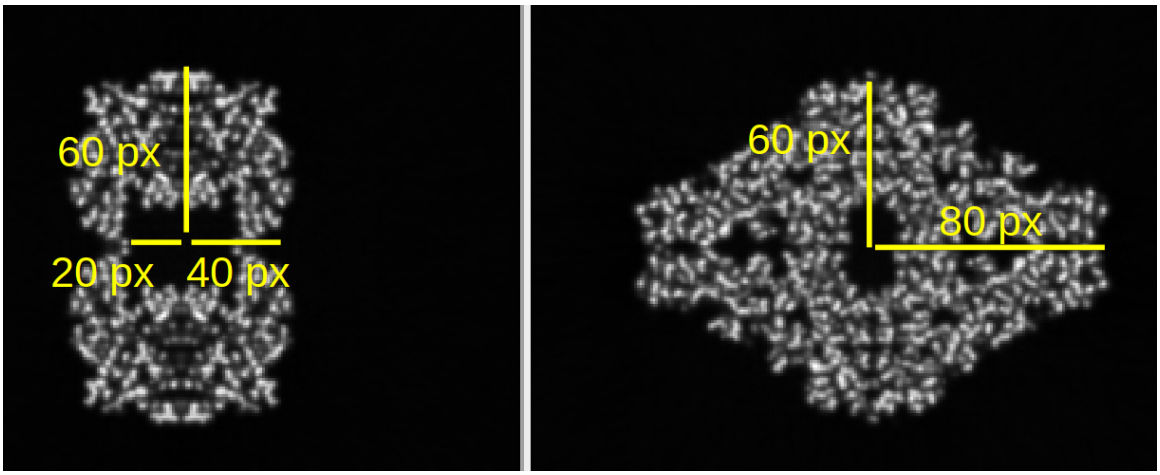

Supplementary Figure 7 – (Supplementary) **Central slices of the $\beta-$galactosidase map** from pdb entry $5a1a$ with the main distances in pixels that determine its geometry.

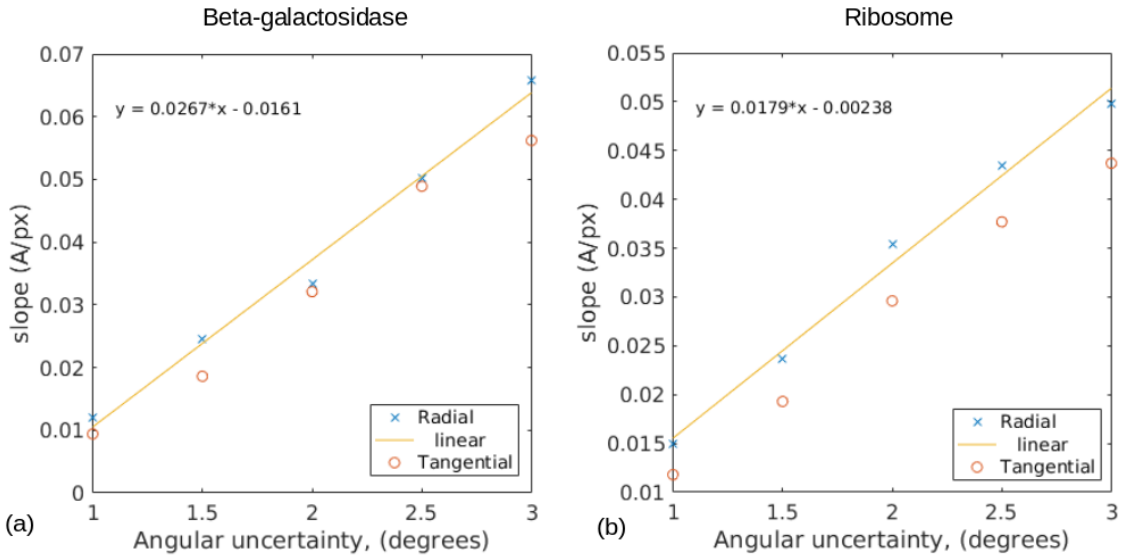

Supplementary Figure 8 – **(Supplementary) Linear fitting of the pairs** (K, σ) for the (a) $\beta-$galactosidase and (b) the Ribosome.